

Effects of Ventricular Myofiber Orientation on Mechanical Function in Human Heart Simulations

Jonathan Krauß, Tobias Gerach, Axel Loewe

Institute of Biomedical Engineering, Karlsruhe Institute of Technology (KIT), Karlsruhe, Germany

Abstract

Currently, personalization of computational human heart models is often performed by combining a carefully designed patient-specific heart geometry with a generic myofiber orientation. This is due to a lack of accurate *in vivo* fiber orientation measurement techniques. In this study, we use a mechanical whole-heart model to evaluate the impact of ventricular fiber angles and sheet angles on clinically relevant mechanical biomarkers of the left ventricle (LV): wall thickening *WT*, mitral valve displacement *MVD*, net LV twist angle ϑ and ejection fraction *EF*. We show that the mechanical function is strongly dependent on the fiber direction. In the evaluated fiber angle configurations, *WT* ranged from 33.38% to 52.48%, *MVD* from 5.85 mm to 18.19 mm and *EF* from 46.83% to 59.95%. For some fiber angles, ϑ was negative. Additionally, ϑ was the only biomarker undergoing significant changes for different sheet angles. For *WT*, *MVD* and *EF* the impact of sheet angle combinations was negligible (< 4.6%), unless changes in the active stress tensor were introduced. Even then, the change between different sheet angle combinations is small compared to the change between different stress tensor formulations. Considering the changes introduced by varying the fiber angles, developing ways of personalizing the fiber orientation or systematically considering its uncertainty appears important.

1. Introduction

Computational models of the human heart can be a valuable research tool and are on the way of clinical adoption. However, before they can be used in a clinical setting, uncertainties of the models have to be evaluated first. One aspect that has a strong influence on mechanical properties is the orientation of the muscle fibers, which dictates the contraction dynamics of the ventricles and atria. Since the fiber orientation is difficult to measure, it is mostly unknown in patients. Fiber angles in the range of 20° to 90° and -90° to 0° are reported in literature for the endocardial and epicardial fibers, respectively [1, 2]. Considering this wide range of reported values, it is critical to understand how the results of human heart simulations depend on the

fiber orientation.

Previous work has shed light on different aspects of the impact of ventricular myofiber orientation. Baron et al. [3] investigated the change in LV stroke volume for six different fiber orientations. They used a constant Δ of 90° between endocardial and epicardial fiber angles. Strocchi et al. [4] focused on atrial dynamics. They evaluated four distinct ventricular myofiber orientations with epicardial fiber angles chosen as the negative value of the corresponding endocardial fiber angle. Both studies did not change the epicardial and endocardial fiber angle independently. Individual measurements by Greenbaum et al. [1] show that neither the assumption of a consistent Δ nor the symmetric angle distribution are physiologically motivated. The fiber angles at the epicardium and endocardium are rather independent. To account for this, we conduct a full factorial simulation study with the endocardial and the epicardial fiber angle as two independent parameters, each of them varied in four equidistant steps of 30° .

Additionally, we investigate three different sheet angle combinations for one reference fiber angle setup. Furthermore, we consider active tension in sheet and/or sheet normal direction leading to a biaxial or triaxial active stress tensor. For all simulations, we evaluate the clinically relevant biomarkers wall thickening, mitral valve displacement, net LV twist angle and ejection fraction.

2. Methods

2.1. Myofiber orientation angles

The myofiber orientation is constructed using the rule-based method suggested by Bayer et al. [5] and modified by Schuler [6]. Four angles are required as input for the algorithm: the fiber angles $\alpha_{\text{endo/epi}}$ at endocardium and epicardium as well as the sheet angles $\beta_{\text{endo/epi}}$. α is defined as the angle between the circumferential axis e_c and the longitudinal fiber direction f in the plane parallel to the myocardial wall. The sheet angle β represents the angle between the transmural axis e_t and the sheet direction s . f and s are perpendicular unit vectors. In combination with the sheet normal n they define the local material coordinate system $\{f, s, n\}$ shown in Figure 1.

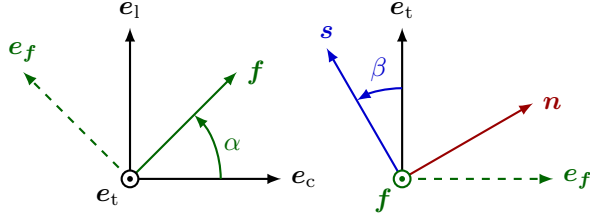


Figure 1. Local material coordinate system $\{\mathbf{f}, \mathbf{s}, \mathbf{n}\}$ derived from local coordinate system $\{\mathbf{e}_c, \mathbf{e}_1, \mathbf{e}_t\}$ with circumferential (\mathbf{e}_c), apicobasal (\mathbf{e}_1) and transmural unit vector \mathbf{e}_t . The longitudinal fiber direction \mathbf{f} (green) is constructed by rotating \mathbf{e}_c around \mathbf{e}_t with the fiber angle α . The transmural unit vector \mathbf{e}_t is then rotated around \mathbf{f} with the sheet angle β to get the sheet direction \mathbf{s} (blue). The sheet normal \mathbf{n} is shown in red.

2.2. Material model

Cardiac mechanics is modeled by solving the governing equation for the balance of linear momentum in total Lagrangian formulation. We assume the myocardium to be hyperelastic and nearly-incompressible as described by Usyk et al. [7] with the parameters $C = 325.56$ Pa, $b_{ff} = 22.0$, $b_{ss} = 8.8$, $b_{nn} = 6.6$, $b_{fs} = 15.4$, $b_{fn} = 13.2$, $b_{ns} = 4.4$ and $k = 1$ MPa.

The 2nd Piola-Kirchhoff stress tensor is additively decomposed into a passive and active component such that $\mathbf{S} = \mathbf{S}_{\text{pas}} + \mathbf{S}_{\text{act}}$ and active tension T_{act} is generated by the model of Niederer et al. [8]. The contraction is initiated by pre-computed activation times based on the solution of the monodomain equation for the reference fiber orientation. Furthermore, boundary conditions including the circulatory system and the pericardium are used as shown in [9]. Parameters were set to achieve physiological conditions in the reference case, where a fiber and sheet angle combination of $\alpha_{\text{endo}} = 60^\circ$, $\alpha_{\text{epi}} = -60^\circ$, $\beta_{\text{endo}} = -65^\circ$ and $\beta_{\text{epi}} = 25^\circ$ was used.

2.3. Mechanical biomarkers

We evaluated clinically relevant mechanical biomarkers of the LV during ventricular contraction, namely LV wall thickening WT , mitral valve displacement MVD , net LV twist angle ϑ and LV ejection fraction EF . Physiological ranges for the evaluated biomarkers are listed in Table 1. Wall thickening WT is given as the percentage change of the mean LV wall thickness $T(t)$ from end-diastole t_{ED} to end-systole t_{ES} :

$$WT = 100 \frac{T(t_{\text{ES}}) - T(t_{\text{ED}})}{T(t_{\text{ED}})} \% . \quad (1)$$

Mitral valve displacement MVD represents the mean displacement of the mitral valve from base to apex:

$$MVD = -(\bar{\mathbf{x}}_{\text{MV}}(t_{\text{ES}}) - \bar{\mathbf{x}}_{\text{MV}}(t_{\text{ED}})) \cdot \mathbf{e}_1 , \quad (2)$$

Table 1. Physiological ranges for the evaluated biomarkers according to literature.

Biomarker	Range	Source
WT	18 .. 100 %	[10]
MVD	12.6 .. 18.8 mm	[11]
ϑ	13 .. 27°	[12]
EF	48 .. 69 %	[13]

with $\bar{\mathbf{x}}_{\text{MV}}$ being the mean of all mitral valve node positions.

The net LV twist angle ϑ is calculated by dividing the LV into segments according to [14] and constructing a basal vector \mathbf{r}_b connecting segments 1 and 4 and an apical vector \mathbf{r}_a connecting segments 13 and 15. Projection onto the $\{\mathbf{e}_t, \mathbf{e}_c\}$ -plane leads to $\hat{\mathbf{r}}_{b/a}$. The rotation angles $\theta_{b/a}(t)$ are calculated as follows:

$$\theta_{b/a}(t) = \text{sgn}(c_{b/a}) \tan^{-1} \left(\frac{\hat{\mathbf{r}}_{b/a}(t) \times \hat{\mathbf{r}}_{b/a}(0)}{\hat{\mathbf{r}}_{b/a}(t) \cdot \hat{\mathbf{r}}_{b/a}(0)} \right) \quad (3)$$

$$c_{b/a} = \hat{\mathbf{r}}_{b/a}(t) \times \hat{\mathbf{r}}_{b/a}(t=0) \cdot \mathbf{e}_1 . \quad (4)$$

The net LV twist angle ϑ is then given by:

$$\vartheta = (\theta_b(t_{\text{ES}}) - \theta_a(t_{\text{ES}})) - (\theta_b(t_{\text{ED}}) - \theta_a(t_{\text{ED}})) . \quad (5)$$

The ejection fraction EF is defined as the percentage change in LV volume $v(t)$ from t_{ED} to t_{ES} :

$$EF = 100 \frac{v(t_{\text{ES}}) - v(t_{\text{ED}})}{v(t_{\text{ED}})} \% . \quad (6)$$

2.4. Design of the simulation study

The simulation study was conducted in a whole heart geometry with 128 976 linear tetrahedral elements [15] and is divided into two parts. The first part focuses on the effect of the longitudinal fiber direction \mathbf{f} for which the fiber angles $\alpha_{\text{endo/epi}}$ were varied independently in four equidistant steps from 0° to $\pm 90^\circ$. The sheet angles were kept constant at $\beta_{\text{endo}} = -65^\circ$ and $\beta_{\text{epi}} = 25^\circ$.

For the second part of the study, we chose the fiber angle combination $(\alpha_{\text{endo}}, \alpha_{\text{epi}}) = (60^\circ, -60^\circ)$ as a reference and varied the sheet angles: $(\beta_{\text{endo}}, \beta_{\text{epi}}) = \{(-65^\circ, 25^\circ); (-25^\circ, 65^\circ); (0^\circ, 0^\circ)\}$. Inspired by Gerach et al. [16], we introduced parameters in the active stress tensor \mathbf{S}_{act} that generate contractile forces perpendicular to \mathbf{f} to consider the full effect of varying sheet angles:

$$\mathbf{S}_{\text{act}} = T_{\text{act}} (\mathbf{f} \otimes \mathbf{f} + K_{ss} \mathbf{s} \otimes \mathbf{s} + K_{nn} \mathbf{n} \otimes \mathbf{n}) . \quad (7)$$

For each sheet angle combination, we investigated four different active stress tensor configurations: $(K_{ss}, K_{nn}) = \{(0, 0); (0.6, 0); (0, 0.6); (0.6, 0.6)\}$.

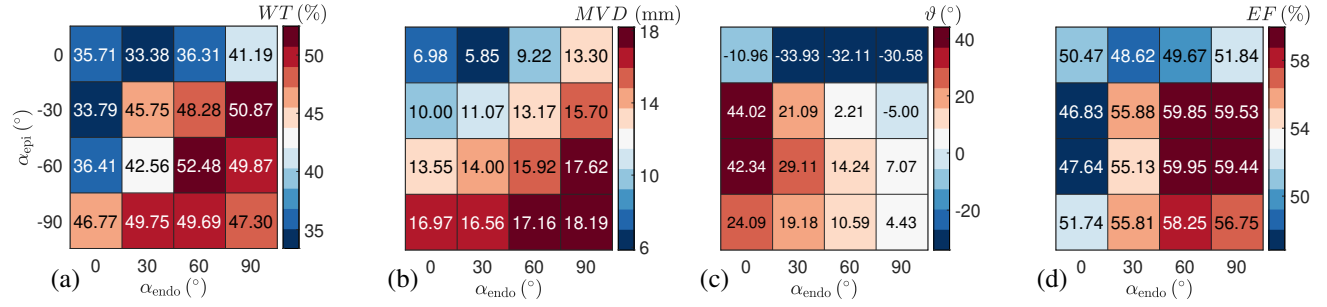


Figure 2. Comparison of wall thickening WT (a), mitral valve displacement MVD (b), net LV twist angle ϑ (c) and ejection fraction EF (d) for different fiber angle combinations ($\alpha_{\text{endo}}, \alpha_{\text{epi}}$).

3. Results

The results for the first part of the simulation study are shown in Figure 2. The maximum values for both WT (52.48%) and EF (59.95%) were observed for the reference simulation ($\alpha_{\text{endo}} = 60^\circ, \alpha_{\text{epi}} = -60^\circ$). This reference fiber angle combination also yielded MVD and ϑ values in their physiological ranges. For some fiber angle combinations ($\alpha_{\text{epi}} = -30^\circ, \alpha_{\text{endo}} = 90^\circ$ and all with $\alpha_{\text{epi}} = 0^\circ$), the apex rotated in the opposite direction resulting in a negative ϑ . MVD ranged from 5.83 to 18.19 mm. Horizontal fibers at either epicardium or endocardium led to lowered WT , MVD and EF . With the exception of two fiber angle combinations, all simulations yielded EF in the physiological range.

Changing sheet angles and the active stress tensor for the reference choice of α led to the results shown in Figure 3. For $K_{ss} = K_{nn}$, the different sheet angle combinations caused only minor differences in all evaluated biomarkers. WT , MVD and EF showed similar behavior for all evaluated sheet angle combinations if the stress tensor was varied. In agreement with the results of WT and EF for a simplified LV model in [16], $K_{ss} = 0.6$ led

to lowered WT , MVD and EF , while $K_{nn} = 0.6$ led to slightly higher or almost unchanged results.

With the exception of ϑ , the differences between the sheet angle combinations for a given active stress tensor were smaller than the changes between the different active stress tensor formulations. This was not the case for ϑ . Here, the sheet angle determined whether introducing a contractile force in sheet direction ($K_{ss} = 0.6$) contributed to ($\beta_{\text{endo}} = -65^\circ, \beta_{\text{epi}} = 25^\circ$) or attenuated ($-25^\circ, 65^\circ$) the twisting motion. With $\beta_{\text{endo}} = \beta_{\text{epi}} = 0^\circ$, the additional force acted in transmural direction and introduced almost no change in the resulting torsion angle.

4. Discussion

All four evaluated biomarkers are strongly dependent on the longitudinal fiber direction f defined by the fiber angles α_{endo} and α_{epi} . Negative values for ϑ can be explained by the way the twisting motion is generated. Negative fiber angles lead to a positive twist. Positive fiber angles lead to a negative twist. If $\alpha_{\text{epi}} = -\alpha_{\text{endo}}$, the epicardial fibers determine the rotation direction as a consequence of the larger radius [17]. For $\alpha_{\text{epi}} = 0^\circ$, the fiber

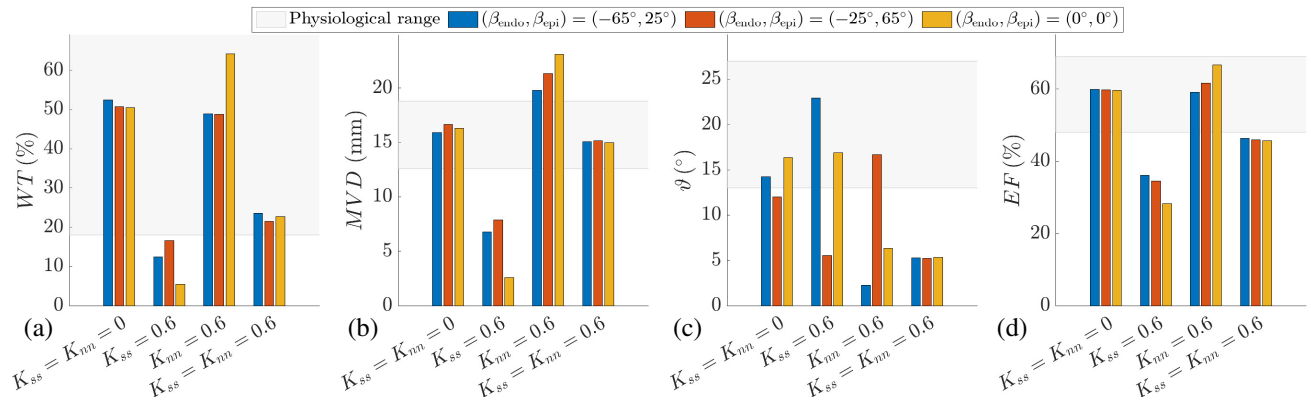


Figure 3. Comparison of wall thickening WT (a), mitral valve displacement MVD (b), net LV twist angle ϑ (c) and ejection fraction EF (d) for different input sheet angle combinations and active stress tensor coefficients. The grey shaded area represents the physiological range for each biomarker. $\alpha_{\text{endo}} = 60^\circ, \alpha_{\text{epi}} = -60^\circ$ for all cases.

angles throughout the myocardial wall are all positive resulting in a negative twist.

In the second part of the study, we found that the sheet angles have a negligible impact on the biomarkers, unless forces in sheet or sheet normal direction are introduced. Even then, for most evaluated biomarkers, the additional force affects the results more than the sheet angle combination. This does not hold for ϑ where the results are largely dependent on the chosen sheet angle combination. This can be explained once again by the way the twisting motion is generated. s and n are perpendicular to f . For $\beta = 0^\circ$, a contraction in n works against the twisting motion at a given point in the myocardial wall. For $\beta = \pm 90^\circ$, the same holds for s . Thus, by introducing $K_{ss} = 0.6$ for $\|\beta_{\text{endo}}\| > \|\beta_{\text{epi}}\|$, the twisting motion at the endocardium is attenuated more than the one at the epicardium leading to an increase of ϑ . For $\|\beta_{\text{endo}}\| < \|\beta_{\text{epi}}\|$ the opposite holds.

This study has several limitations: we focused on ventricular fiber orientation and neglected the impact of atrial fiber orientation changes. In addition, the systematic way of setting up the simulation study leads in part to unphysiological fiber orientations like purely horizontal fibers. Furthermore, we did not take into account the effect of the fibers for the electrophysiology. Specifically, we used a constant activation time map for all simulations, which has been pre-computed for the $(60^\circ, -60^\circ)$ fiber orientation even though the activation times are fiber-dependent.

Considering the changes introduced by varying the fiber angles $\alpha_{\text{endo/epi}}$, developing ways of personalizing the fiber direction f or systematically considering its uncertainty appears important.

Acknowledgments

This project was funded by Deutsche Forschungsgemeinschaft (DFG, German Research Foundation) – LO 2093/6-1 (SPP 2311) and Project-ID 258734477 – SFB 1173.

References

- [1] Greenbaum RA, Ho SY, Gibson DG, et al. Left Ventricular Fibre Architecture in Man. *Br Heart J* 1981;45:248–263.
- [2] Haliot K, Magat J, Ozenne V, et al. 3D High Resolution Imaging of Human Heart for Visualization of the Cardiac Structure. *Lect Notes Comput Sc* 2019;11504:196–207.
- [3] Baron L, Fritz T, Seemann G, et al. Sensitivity Study of Fiber Orientation on Stroke Volume in the Human Left Ventricle. In *Comput Cardiol*, volume 41. 2014; 681–684.
- [4] Strocchi M, Augustin CM, Gsell MAF, et al. The Effect of Ventricular Myofibre Orientation on Atrial Dynamics. *Lect Notes Comput Sc* 2021;12738:659–670.
- [5] Bayer JD, Blake RC, Plank G, et al. A Novel Rule-Based Algorithm for Assigning Myocardial Fiber Orientation to Computational Heart Models. *Ann Biomed Eng* 2012; 40:2243–2254.
- [6] Schuler S. KIT-IBT/LDRB_Fibers, 2021. URL <https://doi.org/10.5281/zenodo.4606575>.
- [7] Usyk TP, Mazhari R, McCulloch AD. Effect of Laminar Orthotropic Myofiber Architecture on Regional Stress and Strain in the Canine Left Ventricle. *J Elasticity* 2000; 61:143–165.
- [8] Niederer SA, Plank G, Chinchapatnam P, et al. Length-Dependent Tension in the Failing Heart and the Efficacy of Cardiac Resynchronization Therapy. *Cardiovasc Res* 2011; 89:336–43.
- [9] Gerach T, Schuler S, Fröhlich J, et al. Electro-Mechanical Whole-Heart Digital Twins: A Fully Coupled Multi-Physics Approach. *Mathematics* 2021;9:1247.
- [10] Sechtem U, Sommerhoff BA, Markiewicz W, et al. Regional Left Ventricular Wall Thickening by Magnetic Resonance Imaging: Evaluation in Normal Persons and Patients With Global and Regional Dysfunction. *AM J Cardiol* 1987;59:145–151.
- [11] Emilsson K, Egerlid R, Nygren BM, et al. Mitral Annulus Motion Versus Long-Axis Fractional Shortening. *Exp Clin Cardiol* 2006;11:302–304.
- [12] Kocabay G, Muraru D, Peluso D, et al. Normal Left Ventricular Mechanics by Two-Dimensional Speckle-Tracking Echocardiography. Reference Values in Healthy Adults. *Rev Esp Cardiol Engl Ed* 2014;67:651–8.
- [13] Petersen SE, Aung N, Sanghvi MM, et al. Reference Ranges for Cardiac Structure and Function Using Cardiovascular Magnetic Resonance (CMR) in Caucasians from the UK Biobank Population Cohort. *J Cardiovasc Magn Reson* 2017;19:18.
- [14] Cerqueira MD, Weissman NJ, Dilsizian V, et al. Standardized Myocardial Segmentation and Nomenclature for Tomographic Imaging of the Heart. *Circulation* 2002; 105:539–542.
- [15] Gerach T, Schuler S, Wachter A, et al. Four-Chamber Human Heart Model for the Simulation of Cardiac Electrophysiology and Cardiac Mechanics, 2021. URL <https://doi.org/10.5281/zenodo.5573921>.
- [16] Gerach T, Schuler S, Kovacheva E, et al. Consequences of Using an Orthotropic Stress Tensor for Left Ventricular Systole. In *Comput Cardiol*, volume 47 of *Comput Cardiol*. 2020; .
- [17] Nakatani S. Left Ventricular Rotation and Twist: Why Should We Learn? *J Cardiovasc Ultrasound* 2011;19:1–6.

Address for correspondence:

Jonathan Krauß, publications@ibt.kit.edu
 Institute of Biomedical Engineering, Karlsruhe Institute of Technology (KIT), Kaiserstr. 12, 76131 Karlsruhe, Germany